Supporting Information

Eggleston et al. 10.1073/pnas.1423294112

Circuit Model Analysis and Enhancement Derivation

In its reduced form, the antenna circuit model, shown in Fig. 3*B*, is fairly simple to analyze. The total Q of the circuit can be found by turning off the source, at which point the circuit simplifies to a simple series RLC circuit with

$$Q=\frac{1}{R}\sqrt{\frac{L}{C_A}\left(\frac{1+\alpha+C_{\mathrm{gap}}/C_A}{\alpha+C_{\mathrm{gap}}/C_A}\right)},$$
$$\omega_0=\sqrt{\frac{1}{LC_A}\left(\frac{1+\alpha+C_{\mathrm{gap}}/C_A}{\alpha+C_{\mathrm{gap}}/C_A}\right)}.$$

The Q is useful to determine the total radiating current, that is, the total current that flows through the radiation resistance. It can be found that

$$I_{\mathrm{rad}}=\frac{I_{\mathrm{o}}Q}{1+\alpha+C_{\mathrm{gap}}/C_A},$$

where I_{o} is the current induced on the antenna by the oscillating optical dipole. It is straightforward to write the total radiated power:

$$P_{\mathrm{rad}}=I_{\mathrm{rad}}^2 R_{\mathrm{rad}}=\left(\frac{I_{\mathrm{o}}Q}{1+\alpha+C_{\mathrm{gap}}/C_A}\right)^2 R_{\mathrm{rad}}.$$

The total antenna efficiency including losses from spreading resistance is then

$$\begin{aligned}\text{Efficiency}&=\frac{P_{\mathrm{rad}}}{P_{\mathrm{rad}}+P_{\mathrm{ohmic}}+P_{\mathrm{spreading}}}\\&=\frac{R_{\mathrm{rad}}}{R_{\mathrm{rad}}+R_{\mathrm{ohmic}}+(I_{\mathrm{o}}/I_{\mathrm{rad}})^2R_{\mathrm{spreading}}}\\&=\frac{R_{\mathrm{rad}}}{R+R^2(C_A/L)\left(\alpha+C_{\mathrm{gap}}/C_A\right)\left(1+\alpha+C_{\mathrm{gap}}/C_A\right)R_{\mathrm{spread}}}.\end{aligned}$$

Now that the radiated power is known, it simply has to be ratioed to the power radiated by a dipole in free space to get the total spontaneous rate enhancement:

$$\begin{aligned}\text{Enhancement}&=\frac{P_{\mathrm{rad}}}{P_0}=\frac{(q\omega_o x_0/d)^2\,Q^2\left(1/\left(1+\alpha+C_{\mathrm{gap}}/C_A\right)\right)^2R_{\mathrm{rad}}}{(2\pi/3)\,Z_o\left((q\omega_0x_o/\lambda_0)\right)^2}\\&=\frac{(\lambda_o/d)^2\left(1/\omega_0^2R^2\right)\left(\left(1+\alpha+C_{\mathrm{gap}}/C_A\right)/\left(\alpha C_A+C_{\mathrm{gap}}\right)\right)^2\left(1/\left(1+\alpha+C_{\mathrm{gap}}/C_A\right)\right)^2R_{\mathrm{rad}}}{(2\pi/3)\,Z_o}\\&=\frac{3}{2\pi}\left(\frac{\lambda_0}{d}\right)^2\frac{\left(1/\omega_o\left(\alpha C_A+C_{\mathrm{gap}}\right)\right)^2R_{\mathrm{rad}}}{Z_0R^2}=\frac{3}{2\pi}\left(\frac{\lambda_o}{d}\right)^2\frac{Z_{\mathrm{gap}}^2\,R_{\mathrm{rad}}}{Z_o(R_{\mathrm{rad}}+R_{\mathrm{ohmic}})^2}.\end{aligned}$$

From this it is clear that a small gap is desired, but not to the point that $C_{\mathrm{gap}} > \alpha C_A$.

Fabrication Process

Antennas were fabricated on an metalorganic chemical vapour deposition (MOCVD)-grown (100) InP epitaxial wafer, using standard semiconductor processing techniques. Processing can be broken down into four main steps: (*i*) alignment mark deposition, (*ii*) InGaAsP ridge formation, (*iii*) antenna deposition, and (*iv*) substrate removal. All lithography was done using e-beam lithography with thin (~80 nm) positive resist.

First, alignment marks consisting of a 5-nm titanium adhesion layer and a 25-nm gold layer were formed using a liftoff process on top of a 35-nm-thick InGaAsP layer. Gold was used because it is resistant to the chemical etching used in later processing steps. Next, thin titanium islands (7 nm thick, 200 nm long, 120 nm wide) were patterned into 20 × 20-μm arrays with a 700-nm staggered pitch and deposited with e-beam evaporation and liftoff. The titanium islands were aligned along crystal planes so that the long axis was parallel to the [011] direction (Fig. S1); these were used as a hard mask to etch ridges into the InGaAsP active layer. A dilute piranha solution (1:8:100 H_2SO_4:H_2O_2:H_2O) was used to slowly wet etch the InGaAsP layer at a rate of ~5 nm/s in the [100] direction, ~2 nm/s in the [011] direction, and ~3.5 nm/s in the [$0\bar{1}1$] direction. Due to the anisotropy of the etchant, the sidewalls parallel to the [011] are fairly vertical for moderate aspect ratios (~1:1). The etching is done in small steps (a few seconds of etching at a time) and then checked under SEM. Because the hardmask layer is so thin, it is semitransparent to the electron beam and the width of the underlying ridge can be determined. Etching continues until the ridge is etched to a width of ~30 nm and then the titanium hardmask is removed with a quick dip in 49% hydrofluoric acid.

Immediately after removal of the titanium hardmask, the sample is loaded into an atomic layer deposition (ALD) machine and pumped down to medium vacuum (~1 Torr). A conformal 3-nm layer of TiO_2 is then deposited on the sample at 150 °C, using ALD. This thin oxide layer provides a uniform surface for all of the ridges and prevents direct contact with the metal antenna deposited in the subsequent step.

Next, 50-nm-wide antennas with lengths varying from 400 nm to 800 nm are patterned perpendicularly over the InGaAsP ridges. A total of 2 nm of germanium is then evaporated at a rate of 0.8 Å/s followed by 40 nm of gold deposited at a rate of 1.5 Å/s. The slow deposition rates yield polycrystalline metal but offer superior conformal coverage compared with quickly evaporated metal. The germanium layer acts as a wetting layer for the gold to ensure connection of the metal arch over the ridge. The metal is then lifted off, leaving the antenna coupled InGaAsP ridges. SEM images are taken at this point to validate successful fabrication of the arch-antenna structure.

After completion of the arch-antenna structure, the entire chip is flipped over and bonded to a glass slide with UV curable epoxy (NOA 81). After UV curing, the epoxy is left to hardbake for 12 h at 50 °C. The InP substrate is then mechanically lapped with fine-

grit sandpaper to a thickness of ∼50 μm. The remaining 50 μm is then etched off with a 1:1 solution of hydrochloric acid:phosphoric acid at 80 °C and stops on a 150-nm-thick InGaAs etch stop layer. The InGaAs layer is removed with a 1:1:10 solution of H_2SO_4:H_20_2:H_20, stopping on a 20-nm InP etch stop layer. This final layer is removed with a 1:1 HCL:phosphoric acid dip, leaving the surface of the epoxy exposed in which the antennas and InGaAsP ridges are embedded.

Total Light Emitted from Antenna Arrays

Arrays (20 μm × 20 μm) of InGaAsP ridges were fabricated with a 700-nm staggered pitch with each array coupled to different length antennas (Fig. S4). To excite carriers in the semiconductor ridges, a Ti:Sapphire laser with a 720-nm center wavelength, a 120-fs pulse width, a 13.3-MHz repetition rate, and 20 μW average power was focused onto the sample, using a confocal microscope setup. The spot size of the pump laser was ∼2 μm and therefore roughly four devices were probed at a time. The pump was polarized in the *y* direction to prevent resonant pumping. Emitted light was collected with the same objective and then filtered with a polarizer to discriminate between light emitted polarized perpendicular (*y* direction) and parallel (*x* direction) to the antenna. Photoluminescence (PL) scans of these arrays (Fig. S4) show the intensity of light emitted polarized in the *x* direction for different length antennas. Enhancement is largest for 400-nm-long antennas, ∼35× stronger than the bare ridge, and slowly decreases with increasing antenna length.

Polarization-Dependent Light Emission

At the nanoscale, geometric dimensions play an important role in emission and absorption properties of semiconductor materials. It is important to note that the bare InGaAsP ridges are slightly polarized even in the absence of metal. Optical emission measurements were taken of bare and antenna-clad ridges to determine the relative ratio of optical emission intensity vs. emission polarization (Fig. S5). Bare ridges preferentially radiate light polarized in the *y* direction compared with the *x* direction by a ratio of 3.3. Previous studies on semiconductor nanowires (1) have shown that this effect can be explained by leaky wave resonances in the nanostructure enhancing *y*-polarized emission.

Surface Recombination

To determine the effect of a thin TiO_2 coating on our InGaAsP surfaces, PL tests were performed on a bare 35-nm InGaAsP layer before and after oxide deposition. The sample was prepared by taking an InP epiwafer with a 35-nm InGaAsP layer and an InP cladding layer grown on top and flip-chip bonding it to a glass slide with epoxy. The substrate was completely removed, leaving the InGaAsP layer exposed to air. Fig. S6 shows the measured PL intensity of the sample under 50-μW illumination from a Ti:Sapphire laser with center wavelength of 1,000 nm. A total of 3 nm of TiO_2 was then deposited on the sample at 150 °C and PL was taken again.

The PL results show an ∼3× decrease in PL intensity after the deposition of TiO_2. Because the sample in both cases is surface recombination limited from the top surface ($\tau_{sr} << \tau_{rad}$), this decrease can be attributed to an ∼3× increase in the surface recombination rate of the top InGaAsP surface once it is exposed to the TiO_2. A similar increase in surface recombination is expected for the patterned ridges during device fabrication. Although this decreases the amount of light emitted, it provides a uniform surface for all cases (bare and antenna coupled) so direct PL comparisons can be done.

1. Cao L, et al. (2009) Engineering light absorption in semiconductor nanowire devices. *Nat Mater* 8(8):643–647.

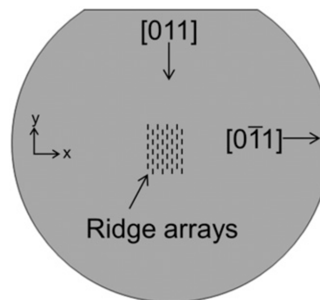

Fig. S1. Schematic of a (100) InP wafer. Shown are crystal directions of the (100) InP epiwafer used for fabrication. Dashes in the center demonstrate the orientation of InGaAsP ridges etched into the wafer (not to scale).

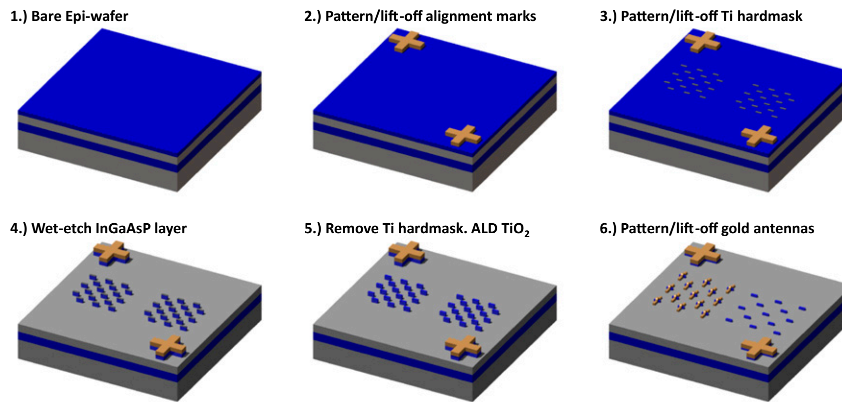

Fig. S2. Arch-antenna fabrication process flow. Shown is the process flow used to etch the InGaAsP ridges and deposit antennas over them.

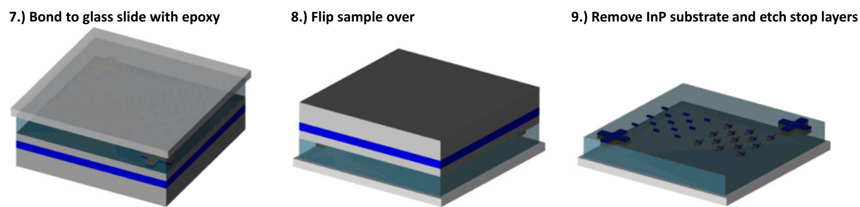

Fig. S3. Flip-chip bonding process flow. Following completion of the arch antenna structures, the chip is bonded to glass with epoxy and the substrate removed.

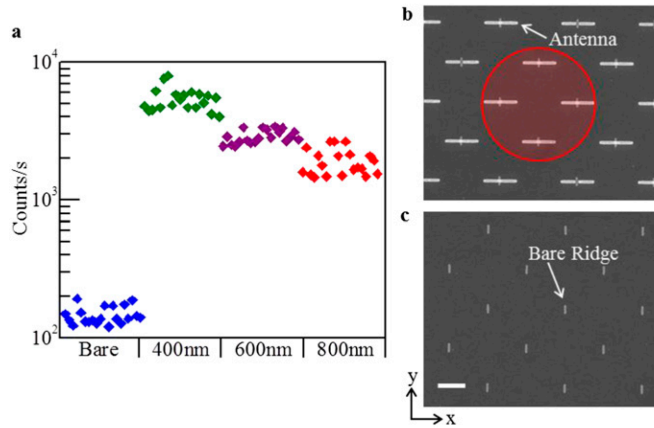

Fig. S4. Integrated photoluminescence parallel to antenna long axis. (*A*) Scatter plot showing PL intensity from the brightest 20 points in a scan of individual 20 × 20-μm InGaAsP ridge arrays coupled to different length antennas. (*B* and *C*) SEM of antenna-coupled and bare ridge arrays. Red circle outlines approximate spot size of pump laser. (Scale bar, 500 nm.)

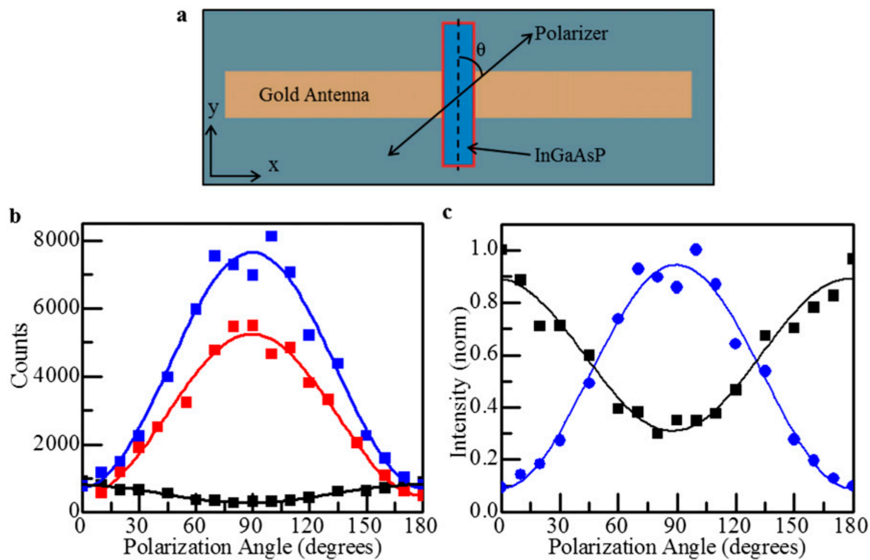

Fig. S5. Polarization dependence of InGaAsP ridges. (*A*) Bottom view of antenna-coupled ridge showing angle of polarizer during measurement. (*B*) Total number of integrated counts for bare ridge (black), 600-nm antenna (red), and 400-nm antenna (blue) as a function of polarizer angle. Symbols are measured data and solid lines are a sinusoid fitting function. (*C*) Normalized intensity of emission from antenna-clad and bare ridge as a function of polarizer angle.

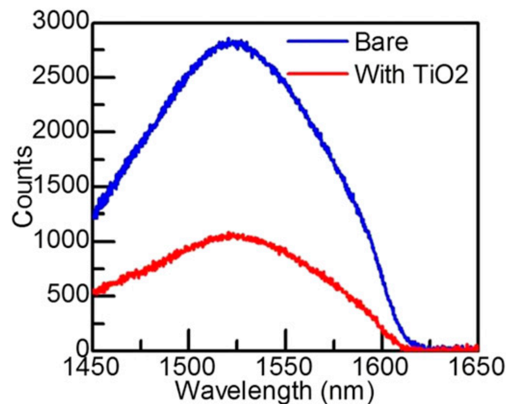

Fig. S6. Photoluminescence of bare InGaAsP layer. Shown is the PL from a bare InGaAsP layer (blue) and the same layer after depositing 3 nm of TiO_2 (red).